

# DNA Polymerase Gamma Acetylation Governs Mitochondrial Homeostasis and Vascular Cell Senescence

Pengbo Wang<sup>1,2#</sup>, Liming Yu<sup>3#</sup>, Kexin Cao<sup>1#</sup>, Xiaofan Guo<sup>1,2#</sup>, Lufan Sun<sup>1#</sup>, Shu Zhang<sup>1,2</sup>, Tong Zhao<sup>1</sup>, Yao Yu<sup>1</sup>, Mengyao Xiong<sup>1</sup>, Chang Liu<sup>1</sup>, Naijin Zhang<sup>1,2</sup>, Yingxian Sun<sup>1,2,4✉</sup>, Guozhe Sun<sup>1,2✉</sup>, Liu Cao<sup>5,6,7</sup>

1. Department of Cardiology, First Hospital of China Medical University, Shenyang City, P. R. China.
2. Health Sciences Institute, China Medical University, Shenyang City, 110122, P. R. China.
3. State Key Laboratory of Frigid Zone Cardiovascular Disease, Department of Cardiovascular Surgery, General Hospital of Northern Theater Command, 83 Wenhua Road, Shenyang City 110016, P. R. China.
4. Key Laboratory of Environmental Stress and Chronic Disease Control and Prevention, Ministry of Education, China Medical University, Shenyang City, P. R. China.
5. Clinical Translational Research Center, Shengjing Hospital, Health Sciences Institute, China Medical University, Shenyang, Liaoning Province, China
6. Innovation Center of Aging Related Disease Diagnosis and Treatment and Prevention, Jinzhou Medical University, Jinzhou, Liaoning, China.
7. Institute of Psychiatry and Neuroscience, Henan Medical University, Xinxiang, Henan, China.

#These authors contributed equally to this work

✉ Corresponding authors: Liu Cao, Clinical Translational Research Center, Shengjing Hospital, Health Sciences Institute, China Medical University, Shenyang, Liaoning Province, China; Innovation Center of Aging Related Disease Diagnosis and Treatment and Prevention, Jinzhou Medical University, Jinzhou, Liaoning, China; Institute of Psychiatry and Neuroscience, Henan Medical University, Xinxiang, Henan, China. Tel: +86 18900911888; E-mail: lcao@cmu.edu.cn. Guozhe Sun, Department of Cardiology, First Hospital of China Medical University; Health Sciences Institute, China Medical University. Shenyang City, P. R. China. Tel: +86 15040292137; E-mail: gzhhsun66@163.com. Yingxian Sun, Department of Cardiology, First Hospital of China Medical University; Health Sciences Institute, China Medical University; Key Laboratory of Environmental Stress and Chronic Disease Control and Prevention, Ministry of Education, China Medical University. Shenyang City, P. R. China. Tel: +86 13804068889, E-mail: yxsun@cmu.edu.cn.

© The author(s). This is an open access article distributed under the terms of the Creative Commons Attribution License (<https://creativecommons.org/licenses/by/4.0/>). See <https://ivyspring.com/terms> for full terms and conditions.

Received: 2025.07.23; Accepted: 2026.01.23; Published: 2026.02.04

## Abstract

DNA polymerase gamma (Poly), the sole polymerase for mitochondrial DNA (mtDNA), emerges as a critical regulator of metabolism-associated senescence. While lysine acetylation represents a key post-translational modification (PTM) influencing mitochondrial function, its mechanistic role in Poly-mediated vascular aging remains undefined. Through combinatorial approaches employing *in vitro* acetylation models and *POLG*<sup>D257A/D257A</sup> mice, a validated model of mitochondrial dysfunction and senescence, we identify Lys 1039 (K1039) as a novel acetylation site which was dynamically regulated during aging process. Both D257A mutation-driven hyper-acetylation of Poly K1039 reduced human aortic smooth muscle cell (HASCs) contractility, triggering pathological hyperproliferation and mitochondrial dysfunction, collectively culminating in premature cellular senescence. Pathological stimulation or genetic manipulation inducing hyperacetylation at K1039 disrupts Poly's binding capacity with mtDNA. This molecular deficiency manifested functionally as compromised contractile performance in HASCs and accelerated senescence phenotypes. Based on the above foundation and *POLG*<sup>D257A/D257A</sup> mice model, we demonstrated that D257A mutation reduced Sirt3-Poly complex formation constituted the pathologically relevant molecular pathway driving aberrant acetylation homeostasis and leading to the senescence. Our findings establish a previously unrecognized regulatory axis wherein Poly acetylation status at K1039 serves as a molecular switch coordinating mtDNA homeostasis, HASCs functionality, and senescence progression. This mechanism might explain the remarkably consistent phenotypic manifestations of Poly-induced dysfunction across diverse tissues and aging models. This work provides fundamental insights into the epigenetic-metabolic crosstalk governing vascular aging processes, providing a unifying framework for age-related vascular pathologies.

Keywords: DNA polymerase gamma, Acetylation, senescence, mitochondrial homeostasis, human aortic smooth muscle cells

## Introduction

Aging of HASMCs, whether through natural aging processes or disease-induced premature senescence, induces characteristic functional deterioration marked by impaired contractile capacity and compromised vascular homeostasis[1-3]. This cellular senescence phenomenon contributes substantially to the global burden of cardiovascular pathologies, representing a critical threat to vascular health. Senescent HASMCs demonstrate profound alterations in metabolic programming, extracellular matrix interactions, and mitochondrial bioenergetics, ultimately manifesting as dysfunctional vascular remodeling[3-5]. While mitochondrial functional integrity is recognized as a central determinant of cellular aging trajectories, current therapeutic strategies targeting terminal effectors like ATP synthase show limited efficacy due to their inability to address upstream regulatory mechanisms[6]. This highlights the need to identify master regulators coordinating mitochondrial homeostasis during senescence.

The *POLG*-encoded Poly serves as the polymerase for mtDNA maintenance. Its polymerase and proofreading activity ensure stable replication of respiratory chain components essential for oxidative phosphorylation[4]. Previous studies confirmed Poly deficiency triggered a cascade of mitochondrial crises including apoptotic activation, oxidative stress amplification, and pathological vascular calcification whose phenomena particularly exacerbated under metabolic stress conditions[7-9]. Emerging evidence suggests Poly may function as a nodal regulator capable of compensating for diverse mitochondrial defects, while most studies predominantly focused on its expression dysregulation in disease [10]. Interestingly, we noted inconsistent expression patterns, even within same disease classifications, which provided the likelihood of alternative Poly activation modalities, such as allosteric or PTM regulation. Protein acetylation modification, a dynamic lysine modification implicated in cardiovascular pathophysiology and aging mechanisms, represents a plausible regulatory pathway given the prevalence of acetylated mitochondrial proteome components[11-14]. However, whether the activity and function of Poly are regulated through acetylation remains incompletely defined.

This work provided the first direct evidence for Poly in PTM, uncovering a previously unrecognized regulatory mechanism through acetylation that governed its functional significance, which mitochondrial genome stability was actively

regulated by acetylation-dependent signaling. Our study identifies K1039 as a novel acetylation site modulating Poly activity in vascular aging. Using the *POLG*<sup>D257A/D257A</sup> mice model of premature senescence with established mitochondrial dysfunction[15, 16], we demonstrated that acetylation at K1039 impairs Poly's DNA-binding capacity, thereby reducing mitochondrial homeostasis and cellular function. We established Poly acetylation as a pivotal regulatory switch in vascular aging, providing a unifying mechanism connecting mitochondrial genomic instability to cellular senescence. The identification of this acetylation-dependent regulatory axis offered novel therapeutic opportunities for targeting age-related cardiovascular pathologies through precision modulation of mitochondrial homeostasis.

## Methods

### Antibodies, reagents and commercial kits

Acetylated-lysine, Cell Signaling Technology (USA) Cat #9441; Citrate Synthase, Santa Cruz (USA) Cat #sc-6246; COX IV, Wanleibio (China) Cat #WL01418; Flag-tag, Absmart (China) Cat #M20008; Flag-tag, GNI (Japan) Cat #GNI4110-FG-M; GAPDH, Proteintech (China) Cat #60004-1-Ig; GCN5, Proteintech (China) Cat #66575-1-Ig; HRP goat anti-mouse IgG, ABclonal Biotech Cat #AS003; HRP goat anti-rabbit IgG, ABclonal Biotech Cat #AS014; L-type  $\text{Ca}^{2+}$  CP, Santa Cruz (USA) Cat #sc-515679; Myc-tag, Cell Signaling Technology (USA) Cat #2276; p16, Proteintech (China) Cat #10883-1-AP; p16, Wanleibio (China) Cat #WL02203; p21, Santa Cruz (USA) Cat #sc-6246; PKM2, Cell Signaling Technology (USA) Cat #4053S; PKM2-phosphorylation, Cell Signaling Technology (USA) Cat #3827S; Poly, Abcam (USA) Cat # ab128899; Poly, Abcam (USA) Cat # ab97661; Poly, Cell Signaling Technology (USA) Cat #13609; Poly, Santa Cruz (USA) Cat #sc-390634; Sirt3, Santa Cruz (USA) Cat #sc-6246; TRPC6, Santa Cruz (USA) Cat #sc-515837; Tubulin, Proteintech (China) Cat #11224-1-AP.

FBS, Clark (Australia) Cat #FB15015; High-glucose DMEM, Biological Industries (Israel) Cat #01-052-1A; High-fat Diet Feed, Medicience (China) Cat #MD12033; HiGene, Applygen (China) Cat #C1506; Lipofectamine 2000, Thermo Scientific (USA) Cat #11668019; NAM, MedChemExpress (USA) Cat #HY-101407; PageRuler<sup>TM</sup> Multicolor High Range Protein Ladder, Thermo Scientific (USA) Cat #26625; PageRuler<sup>TM</sup> Prestained Protein Ladder, Thermo Scientific (USA) Cat #26616; Protein A/G Magnetic Beads, Selleckchem (USA) Cat #B23202; Sirt3 activator, MedChemExpress (USA) Cat #HY-139742; Sirt3 inhibitor, MedChemExpress (USA)

Cat #HY-108331; Streptozotocin, MedChemExpress (USA) Cat #HY-13753; TSA, MedChemExpress (USA) Cat #HY-15144; Type I Collagen Solution, Solarbio (China) Cat #C8062; Vit D<sub>3</sub> solution, Solarbio (China) Cat #V8070; Cell Counting Kit-8, Beyotime (China) Cat #C0037; Chromatin IP Kit, Merck (USA) Cat #17-10086; JC-10 Assay Kit, Solarbio (China) Cat #CA1310; Mitochondrial Extraction Kit, Solarbio (China) Cat # SM0020; SA-B-Gal Staining Kit, Beyotime (China) Cat #C0602; SimpleChIP® Enzymatic Chromatin IP Kit (Magnetic Beads), Cell Signaling Technology (USA) Cat #9003.

### Mouse models

The *POLG*<sup>D257A/D257A</sup> mice were generously provided by Professor Nils-Göran Larsson. Wild-type (WT) littermates *POLG*<sup>WT/WT</sup> mice and C57/BL6 WT mice served as controls. All mice were maintained under specific pathogen-free conditions at 21–23°C with ad libitum access to standard chow and distilled water. Animal protocols were approved by the Institutional Animal Care and Use Committee (IACUC) of China Medical University and conducted in compliance with NIH guidelines (Publication No. 85-23, revised 1985).

For vascular calcification induction, mice received subcutaneous injections of vitamin D3 (8×10<sup>5</sup> IU/kg in corn oil) daily for 3 days and were euthanized on day 12[7]. To model diabetic vascular injury, mice were fasted for 5 days, administered streptozotocin (40 mg/kg, intraperitoneal), and maintained on a high-fat diet for 6 weeks[17].

### Cell lines and cell culture

HASMCs and HEK293T cells were generously provided by Professor Liu Cao. Sh-Poly HASMC lines were generated as previously described[7]. Cells were cultured in high-glucose Dulbecco's modified Eagle's medium (DMEM) supplemented with 10% FBS, 100 U/mL penicillin, and 100 µg/mL streptomycin at 37°C under 5% CO<sub>2</sub>.

### Mouse embryonic fibroblasts (MEFs) and primary HASMC isolation

MEFs were isolated from E12.5 fetal skin tissues. Tissues were digested with EDTA-free trypsin (0.25%, w/v), and cells were cultured in DMEM containing 15% FBS at 37°C with 5% CO<sub>2</sub>. Primary HASMCs were isolated from 8-week-old murine thoracic aortae. Following microdissection to remove adventitial connective tissue and the tunica intima, the aortic tunica media layer was isolated, mechanically minced, and subjected to enzymatic digestion with EDTA-free trypsin (0.25%, w/v) to dissociate smooth muscle cells, and cells were

cultured in DMEM containing 15% FBS at 37°C with 5% CO<sub>2</sub> for downstream functional analyses.

### Mass spectrometry acetylation modification omics

Samples preparations were following standard procedures for acetylation modification omics analysis. Acetylated peptides were enriched using iTRAQ labeling and anti-acetyl-lysine antibody-conjugated agarose beads. After 1-hour incubation at 4°C, peptides were eluted and analyzed by LC-MS/MS. Spectral counting quantified acetylation levels.

### Western blot (WB) and co-immunoprecipitation (Co-IP) analysis

Cells or tissues were lysed on ice (30 min) and vortexed every 10 min, centrifuged (13,000 ×g, 20 min), and quantified. Lysates (30–50 µg) were resolved on 8% or 12% SDS-PAGE gels, transferred to PVDF membranes (80 V, 150 min), and blocked with 5% non-fat milk or BSA blocking solution. Primary antibodies (1:200-1,000 dilution) were incubated overnight at 4°C, followed by HRP-conjugated secondary antibodies (1 h, RT). Chemiluminescent signals were quantified using ImageJ v1.46 (National Institutes of Health, USA <https://imagej.nih.gov/ij/>), normalized to Tubulin or GAPDH. For Co-IP, lysates were incubated with antibodies (3 h, 4°C), followed by protein A/G beads (12 h, 4°C). Precipitates were analyzed by WB.

### Chromatin immunoprecipitation (Ch-IP) analysis

Ch-IP assay was performed according to the manufacturer's protocols. In brief, prepared samples were cross-linked with 1% formaldehyde at room temperature for 10 minutes and chromatin was lysed into fragments with sonication following addition of Glycine for 5 minutes. Then the samples were incubated with complex of primary antibodies and protein A/G beads overnight at 4°C. On the next day, immunoselected DNA fragments were purified after the beads-antibody-DNA fragment complex was collected and reverse cross-linked. Finally, DNA fragments were used for qPCR experiments. Forward Primer for Ch-IP, CTGAGCTCACCATAGTCTAATAG; Reverse Primer for Ch-IP, GATGTTGGATGTAAAGTGAAAT; The results of Ch-IP analysis were exhibited as percentage of input chromatin and were derived from a single experiment that is representative of at least three independent experiments.

## Subcellular component isolation

Mitochondria were isolated from freshly collected cells using a mitochondrial extraction kit. First, the cells were ground with a glass grinder and then broken with lysis buffer. The samples were centrifuged at 1000 g for 5 min at 4 °C, twice, and then centrifuged at 12,000 g for 10 min. The supernatant was collected as cytoplasmic protein. Then wash the pellets with wash buffer and centrifuged at 12,000 g for 10 min at 4 °C. The precipitate was collected as mitochondria.

## Co-localization analysis

The cell slides were placed into 24-well plates with clean forceps, and then the cells were cultured. When the cells grew to 70-80% density, the cell culture-medium was discarded and washed with PBS. Precooled methanol solution was used for fixation at room temperature for 3min, followed with three times washing with PBS. Then the slides were drilled with 0.25%Triton-100 for 15min at room temperature and washed with PBS at the end. After that, the cells were blocked with 5% BSA solution at room temperature for 1 hour, and 300ul of primary antibody in 5% BSA solution was added. The cells were incubated overnight at 4 °C. The next day the plates were washed with PBS, and then were incubated with fluorescent secondary antibodies at room temperature for 1h in the dark place. After the incubation, the cells were washed with PBS again and the DAPI solution was used to stain the nuclei. Then wash the cells again with PBS, and the slides were placed on microscope slides and sealed with antifade mounting medium. Fluorescence co-localization was observed and photographed using a confocal microscope at 40x magnification. The mean fluorescence intensity was calculated using Image J for comparison between groups.

## Plasmid construction and transfection

The methods of constructing Poly-WT plasmid and Poly-D257A plasmid has been described in previous articles[7]. In this study, the PCR technology was used to construct point mutation plasmids. We made exogenous gene expression by transfection[18]. Transfection was performed when the cells had grown to 60% confluence. The transfection mixture containing plasmid (10 $\mu$ g DNA for each plasmid in a 10cm cell culture dish, the vector plasmid was used as control group), transfection reagent Lipofectamine 2000 or HiGene and PBS was placed at 37 °C for 15min after thorough mixing, and then it was added to the cell culture medium. The medium was changed after 6 hours, and the cells were collected after 48 hours for the following analysis experiments.

## Cell viability assay

We used Cell Counting Kit-8 (CCK-8) to evaluate the cell viability. The treated cells were inoculated into 96-well plates with 8000 cells for each well and incubated in incubator. On the next day, 10  $\mu$ l of CCK-8 solution was added to each well and incubated for 90 min in the incubator. Detect the absorbance at 450 nm to evaluate the proliferative ability and activity of the cells.

## Colony forming assay

The digested cells were counted and cultured into 6cm cell culture dishes with 3000 cells per dish. The cells were cultured with DMEM for 7 days, and the medium was changed every two days. Staining and photography were performed on day 0/3/7, respectively. Before staining, the medium was dropped, the cells were fixed with paraformaldehyde at room temperature for 15min, and then washed it with PBS. 0.1% crystal violet staining solution was used for staining at room temperature for 15min. After staining, the non-specific staining was washed away with PBS. Taking photograph under the microscope, a colony was defined as more than 50 cells. The colonies were counted by Image J, and colony formation rate was calculated.

## SA- $\beta$ -Gal staining

We performed SA- $\beta$ -Gal staining to observe the senescent level of cells. After discarding the culture medium and washing the cell surface with PBS solution, we fixed the cells with paraformaldehyde at room temperature for 15 minutes. After fixation, the cell fixative was aspirated and the cells were washed with PBS three times, each time for 3 minutes. The prepared staining solution was added to the culture dish and the culture dish was sealed and then placed in a 37°C incubator without CO<sub>2</sub> overnight. On the next day, we discarded the staining solution and added 2 milliliters of PBS. The staining was observed under a microscope and photographs were taken. The ImageJ was used to count the proportion of color-positive cells in the field as a measure of the degree of aging.

## Collagen gel contraction assays

We conducted collagen gel contraction experiment to observe the contraction ability of HASMC. The cells were digested, counted and then diluted into a single-cell suspension. We mixed 300  $\mu$ l of cell suspension, 100  $\mu$ l of type I collagen solution, 94  $\mu$ l of DMEM, and 6  $\mu$ l of NaOH solution carefully on ice. The prepared cell gel was seeded in a 24-well plate and placed in a 37°C incubator for 30 minutes. After gel formation, 500  $\mu$ l of culture medium was

added to each well and the gel was gently detached from the well walls. Then the plate was incubated in a 37°C incubator. The photographs were taken using a gel imaging system at 0 hours and 12 hours after gel formation, and the surface area of the collagen gel was measured using ImageJ software. The percentage of gel surface area contraction (%) was calculated using the formula: [(0h area - 12h area) / 0h area] × 100%.

### Mitochondrial membrane potential (MMP) determination

We used JC-10 assay kit to determine the MMP and further evaluate the mitochondrial function. We digested the cells and resuspended them into a single-cell suspension using culture medium. The prepared JC-10 staining solution was added and mixed thoroughly. Then the cells were incubated in a light-protected cell culture incubator at 37°C for 20 minutes. After incubation, the cells were centrifuged at room temperature. Then we aspirated supernatant and washed cells twice with PBS solution, followed by adding 2 mL of culture medium to resuspend into a single-cell suspension, and the MMP was analyzed using flow cytometry with FITC and PE channels. The ratio was calculated to evaluate the MMP and mitochondrial function.

### Molecular modeling

We used SWISS-MODEL (<https://www.swissmodel.expasy.org>) to model the three-dimensional (3D) structural coordinates of Poly to provide molecular structure evidence for our hypothesis which D257A mutation might bring alteration in acetylation modification and protein binding levels. The amino acid sequence of Poly was obtained from the NCBI database and the sequence was submitted to the SWISS-MODEL web server to generate the models based on query sequence coverage and identity. We used the Global Model Quality Estimation (GMQE) and Qualitative Model Energy Analysis (QMEAN) values accessing system to guarantee the reliability of 3D structure, and we eventually selected the model with the highest GMQE value and the QMEAN value below 4.0.

### AlphaFold-structure prediction

To predict the structural consequences of lysine acetylation, we employed AlphaFold3 for protein structure modeling. The WT Poly sequence was submitted to AlphaFold3 to generate a baseline structural model. To simulate acetylated lysine residues, we introduced acetyl-lysine analogs at specified positions (K1039) by modifying the residue type in the input sequence using a structural parameter set compatible with the CHARMM36 force

field. Five models were generated for each variant, and the model with the highest predicted confidence score was selected for further analysis. Structural comparisons between wild-type and acetylated forms were performed by aligning the predicted models in PyMOL (version 2.5.4).

### Molecular docking

The protein structures of Poly (WT and D257A) and Sirt3 were obtained from AlphaFold-predicted models. These structures were downloaded and converted into the GROMACS-specific format (.gro) using GROMACS software (version 2022.5). During this conversion process, missing atoms were repaired, and defects in terminal residues were ignored to ensure the completeness of the structure files and the accuracy of subsequent simulations. To simulate the dynamic behavior of Poly (WT and D257A) and Sirt3 under physiological conditions, a solvated system was constructed using GROMACS modules, including editconf, solvate, and genion. The proteins were placed in a water box, and counter-ions were added to ensure system neutrality. The system underwent two stages of equilibration: NVT (constant volume constant temperature) to stabilize the temperature while maintaining a constant volume, and NPT (constant pressure constant temperature) to stabilize the pressure and mimic physiological conditions. Molecular docking was performed using ClusPro 2.0 (<https://cluspro.bu.edu/>), where docking simulations of Poly (WT and D257A) and Sirt3 proteins with small molecules (both modified and unmodified) were conducted. The docking pose with the lowest binding energy, indicating the highest binding affinity, was selected as the final result.

### Quantification and statistical analysis

The data are presented as mean ± SD. The F-test (two groups) or the Brown-Forsythe test (three or more groups) was used to assess the homogeneity of variance. The Shapiro-Wilk test was used to assess the normality of the data. Student's t-test and Welch's t-test were used for equal variance and unequal variance, respectively (two groups). Two-way analysis of variance with the Bonferroni multiple-comparisons test was used when two conditions were considered between the groups. The p values were adjusted for multiple comparisons where appropriate. GraphPad Prism 8.0 software, SPSS version 22.0 (IBM Corp., Armonk, NY, USA <https://www.ibm.com/spss>) and R software (version 4.0.5 <http://www.R-project.org>) were used for all statistical analyses, with a P value less than 0.05 indicating statistical significance.

## Results

### Poly could undergo acetylation and is augmented in senescent HASMC

Previous studies established that the D257A mutation in Poly induces premature aging phenotypes in mice, including shortened lifespan, spinal deformities, and alopecia (Figure 1A). Given the regulatory role of acetylation in protein function, we observed a hyper-acetylated state in mitochondrial proteins of aged mice (Figure 1B). Co-immunoprecipitation (Co-IP) assays confirmed Poly acetylation, which was further enhanced by deacetylase inhibitors TSA/NAM (Figure 1C). We also performed physiological aging model, vascular calcification model and diabetes model, and we observed the expression of senescent marker p16 and p21 were elevated in all three models which indicated these common pathological models were all accompanied with senescence process (Figure 1D, E). Furthermore, the respectively Co-IP experiment indicated the acetylation of Poly were all up-regulated in these senescent models, suggesting the acetylation of Poly could be regulated and involved into different aging related processes (Figure 1F-J). Based on the above results, we compared *POLG*<sup>D257A/D257A</sup> mice with *POLG*<sup>WT/WT</sup> mice and observed Poly-D257A exhibited a higher acetylation level which was also confirmed *in vitro* (Figure 1K-M).

These results demonstrated Poly could undergo acetylation modification which could be dynamically regulated during senescence and contributed to D257A mutation-induced aging. Based on these findings, we proposed that Poly integrated diverse senescence-inducing signals, whether arising from genetic deficiency, physiological processes or pathological conditions, and transduced senescence-related effector signals through modulation of its acetylation status (Figure 1N).

### D257A mutation elevated acetylation level, reducing HASMCs function and disrupting the mitochondrial homeostasis

To reveal the role of Poly D257A mutation in HASMC function and senescence process, we compared the difference among *POLG*<sup>WT/WT</sup> mice, *POLG*<sup>D257A/D257A</sup> (homozygote mice, HO) mice and senescent *POLG*<sup>D257A/D257A</sup> mice. In *POLG*<sup>D257A/D257A</sup> mice, p16/p21 expression were markedly elevated, worsening with age (Figure 2A). In the proliferative aging model, we performed the SA- $\beta$ -gal staining and indicated the *POLG*<sup>D257A/D257A</sup> MEFs of P3 has already exhibited senescence and further aggravated in P7 (Figure 2B). Concurrently, Poly acetylation increased progressively in *POLG*<sup>D257A/D257A</sup> mice and further

aggravated with age (Figure 2C). Functional assays revealed impaired contractility in Poly-mutant HASMCs which even lost contraction ability in senescent HASMCs (Figure 2D, E), linked to reduced L-type  $\text{Ca}^{2+}$  channel (LCP) and TRPC6 expression which were important influx  $\text{Ca}^{2+}$  marker and essential for maintain the contractive ability (Figure 2F). Paradoxically, *POLG*<sup>D257A/D257A</sup> HASMCs exhibited hyperproliferation via Cell Counting Kit-8 (CCK8) assay and colony formation assays no matter they were young or senescent suggesting a abnormal high proliferation rate (Figure 2G, H). And we noted the D257A mutation attenuates senescence-associated decline in proliferative capacity, as evidenced by the robust proliferative capability of Passage 9 (P9) D257A HASMCs which remained comparable to that of P3 WT HASMCs (Figure 2I). Finally, we also examined mitochondrial function and found that the D257A mutation diminished mitochondrial membrane potential (MMP) levels, which further worsened with aging (Figure 2J). Mitochondrial dysfunction was also evident through suppressed citrate synthase (CS), and elevated pyruvate kinase isozyme type M2 (PKM2) phosphorylation in *POLG*<sup>D257A/D257A</sup> HASMCs and even more obvious in senescent cells, indicating a metabolic shift toward glycolysis (Figure 2K).

Herein, we observed D257A mutation driven senescence via disrupted mitochondrial homeostasis and aberrant HASMC function which were diminished contraction ability and hyperproliferation. HASMCs maintained a dynamic balance between contractile phenotype and proliferative phenotype. This "phenotypic equilibrium" shifted toward either phenotype in response to microenvironmental alteration. Pathologically, however, HASMCs would develop hyper-contractile phenotypes associated with apoptosis and pathological vascular remodeling, or undergo hyper-proliferation-driven premature senescence (Figure 2L). Critically, D257A mutation mediated Poly acetylation might be the effect process which disrupted phenotypic balance of HASMCs which further leading to senescence.

### The acetylation modification of Poly is mediated by GCN5/Sirt3

To delineate the molecular pathways governing Poly acetylation, we systematically screened acetyltransferases and deacetylases regulating this post-translational modification. After overexpressing common acetyltransferases to HASMCs, acetyltransferase screening identified GCN5 as the primary enzyme mediating Poly acetylation, validated by endogenous Co-IP and colocalization assay (Figure 3A-C). Meanwhile, we observed GCN5

significantly improved the acetylation level of Poly (Figure 3D). The above results suggested that GCN5 was the acetyltransferase of Poly. Next, we enriched Poly protein and conducted mass spectrometry acetylation modification omics, the results pinpointed K1039 site which was highly conserved among several species might undergo acetylation (Figure 3E-F). Thus, we confirmed whether K1039 was the

acetylation site of Poly by acetylation deficiency mutation. By transfecting Poly-WT plasmid and Poly acetylation-deficiency plasmid (Poly-K1039R), we observed that Poly-WT had appropriate basal level acetylation modification, K1039R mutation reduced acetylation modification, these results confirmed this site's role in modulating acetylation levels (Figure 3G).

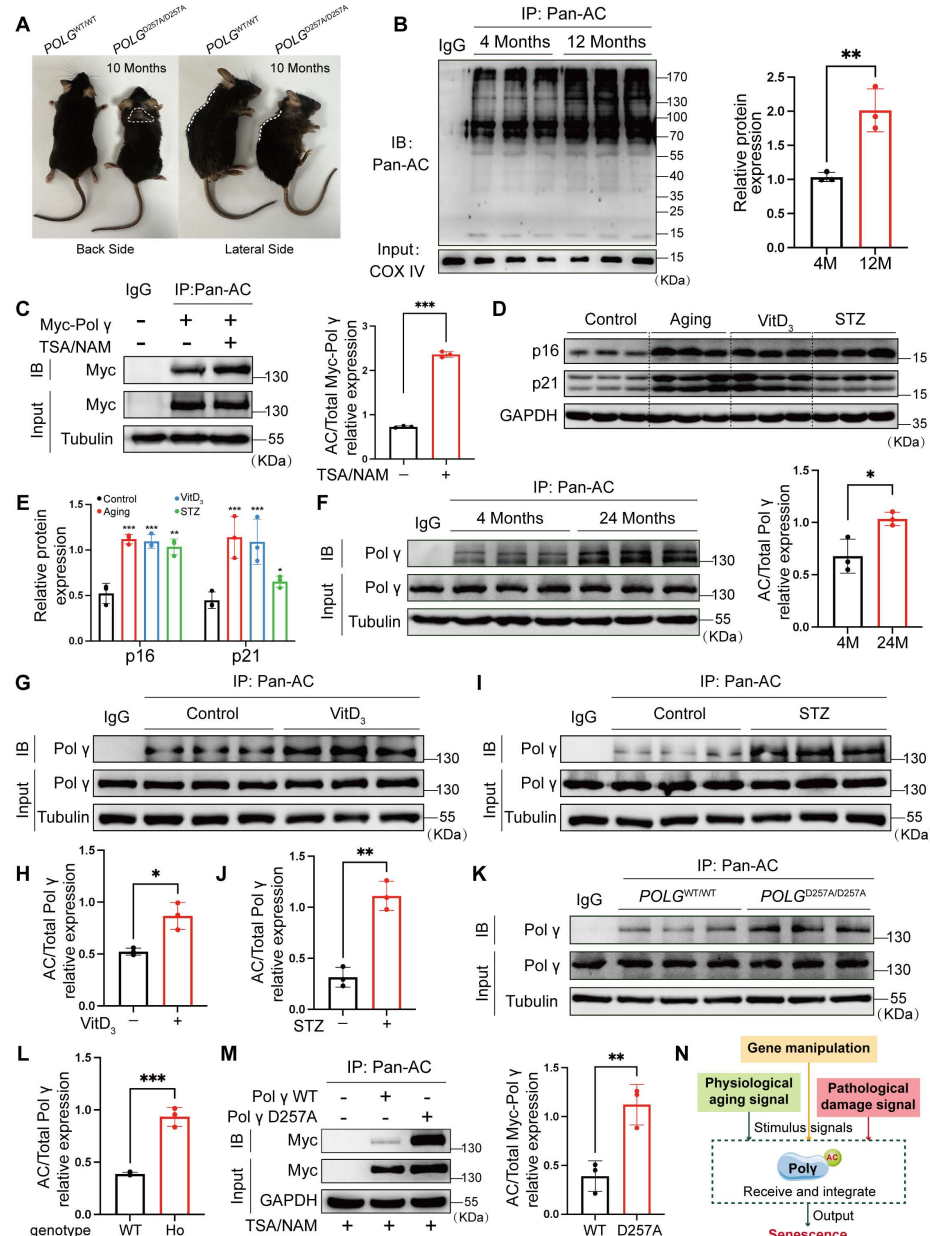


**Figure 1. Poly acetylation is augmented during senescence and regulated by D257A mutation.** (A) The difference of morphological characteristics between *POLG*<sup>WT/WT</sup> mice and *POLG*<sup>D257A/D257A</sup> mice; (B) The global acetylation of mitochondrial protein among different age in mice aorta by Co-IP assay, the right panel is the quantification analysis. COX IV was used as a loading control, \*\* $p < .01$ ; (C) Co-IP analysis and quantification (right panel) of relative acetylation level of Poly in HASMCs which treated with TSA/NAM for 24 hours. The expression of Myc in input was used as a loading control, \*\*\* $p < .001$ ; (D, E) The molecular marker expression of senescence in aging model, vascular calcification model and diabetes model by WB assay and its quantification analysis. The expression of GAPDH was used as a loading control, \*\*\* $p < .001$ , \*\* $p < .01$ , \* $p < .05$ ; (F-J) The acetylation of Poly in different models by Co-IP assay and their quantification analysis. (F) for 4 months and 12 months mice aorta, (G, H) for control and  $\text{VitD}_3$  induced vascular calcification model and (I, J) for control and STZ induced vascular diabetes model. The expression of Poly in input was used as a loading control, \*\*\* $p < .001$ , \* $p < .05$ ; (K, L) The acetylation of Poly in aorta of *POLG*<sup>WT/WT</sup> mice and *POLG*<sup>D257A/D257A</sup> mice by Co-IP assay and its quantification analysis. The expression of Poly in input was used as a loading control, \*\* $p < .01$ ; (M) Transfect the HASMCs with Vector plasmid, Poly-WT plasmid and Poly-D257A plasmid for 48 hours respectively, and detect their acetylation level by Co-IP assay. The right panel is the quantification analysis. The expression of Myc in input was used as a loading control, \*\* $p < .01$ ; (N) Schematic diagram. All data were expressed as the mean  $\pm$  SD of triplicate experiments. In each independent experiment, the sample size for each group of experiments is 3.

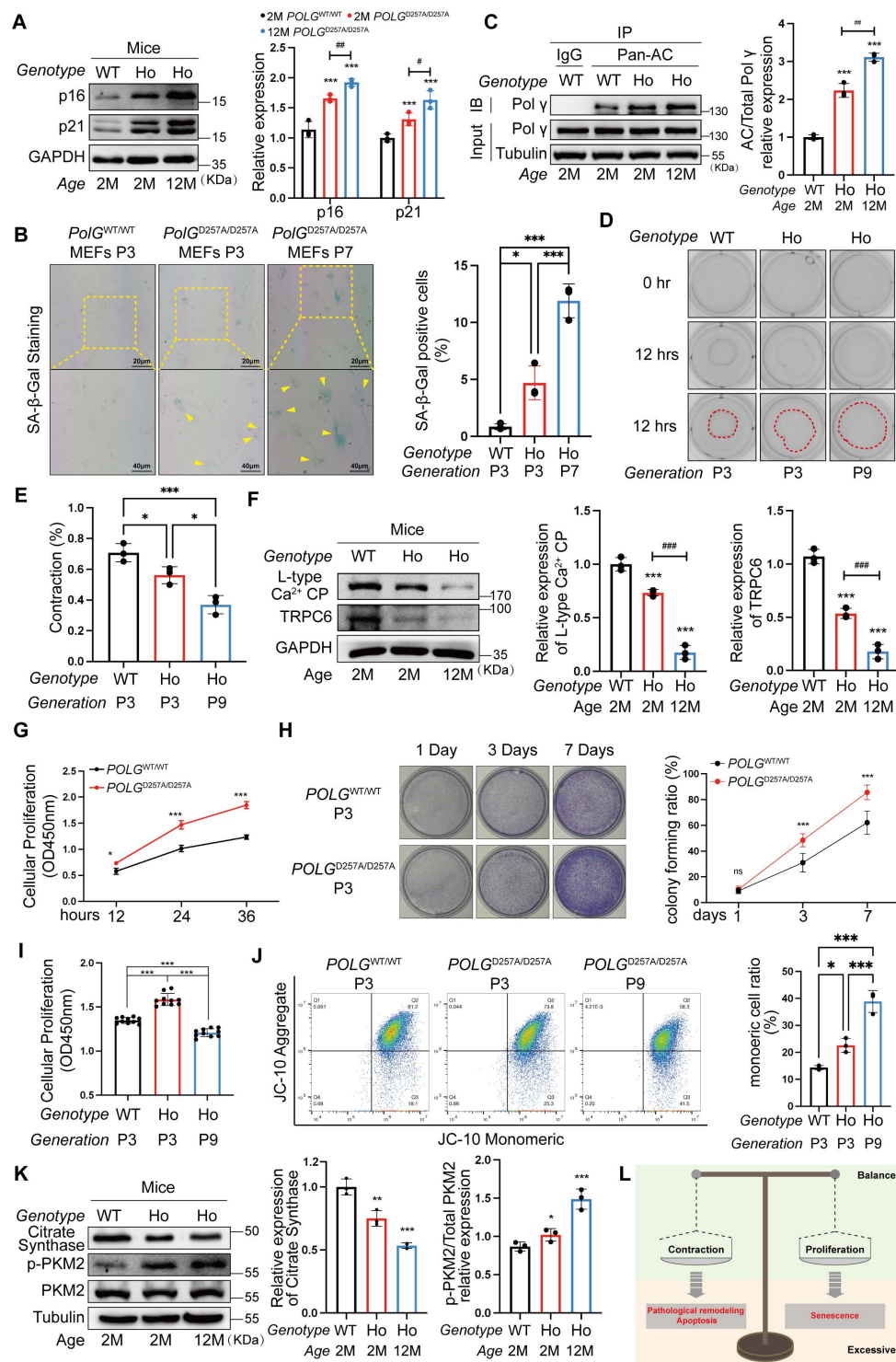


**Figure 2. D257A mutation exacerbates senescence via dysregulated HASMC function and mitochondrial dysfunction.** (A) The different expression of senescence marker in the aorta of *POLG*<sup>WT/WT</sup> mice and *POLG*<sup>D257A/D257A</sup> mice by WB assay, the right panel is the quantification analysis. WT is for *POLG*<sup>WT/WT</sup> mice and HO is for *POLG*<sup>D257A/D257A</sup> mice. The expression of GAPDH was used as a loading control. \*\*\*p < .001, #p < .01, \*p < .05; (B) SA- $\beta$ -Gal staining for MEFs with different genotype and passage. The rate of positive staining cells was counted to analysis. \*\*\*p < .001, \*p < .05; (C) Co-IP analysis and quantification analysis of relative acetylation level of Poly in aorta of different genotype and age. \*\*\*p < .001, #p < .01; (D-E) The collagen gel contraction experiment of primary HASMCs with different genotype and passage. The percentage of gel surface area contraction (%) was calculated using the formula: [(0h area - 12h area) / 0h area]  $\times$  100%. \*\*\*p < .001, \*p < .05; (F) The expression of various  $\text{Ca}^{2+}$  channel related proteins in aorta of *POLG*<sup>WT/WT</sup> mice and *POLG*<sup>D257A/D257A</sup> mice by WB assay, the median and right panels are quantification analysis. The expression of GAPDH was used as a loading control. \*\*\*p < .001, #p < .001; (G) The cell viability experiment of primary HASMC of *POLG*<sup>WT/WT</sup> mice and *POLG*<sup>D257A/D257A</sup> mice by CCK-8 kit assay in 12 hours, 24 hours and 36 hours. \*\*\*p < .001, \*p < .05; (H) The colony forming experiment of primary HASMC of *POLG*<sup>WT/WT</sup> mice and *POLG*<sup>D257A/D257A</sup> mice, the cells were cultured for 7 days, staining and counting the colony numbers in 1 day, 3 days and 7 days. Counting the colony numbers to analysis. \*\*\*p < .001, \*p < .05, ns p>0.05; (I) The cell viability experiment of primary HASMC of *POLG*<sup>WT/WT</sup> mice and *POLG*<sup>D257A/D257A</sup> mice with different passage by CCK-8 kit assay in 12 hours, 24 hours and 36 hours. \*\*\*p < .001, \*p < .05; (J) The JC-10 measurement of MMP of the primary HASMC of different genotype and passage by flow cytometry. Compare the difference of monomeric cells ratio (green) in every subgroup. \*\*\*p < .001, \*p < .05; (K) The expression of metabolic proteins (citrate synthase, p-PKM2, PKM2) in aorta of different genotype and age. The expression of Tubulin was used as a loading control for citrate synthase, and PKM2 was used as a loading control for p-PKM2. The median and right panels are quantification analysis. \*\*\*p < .001, \*\*p < .01, \*p < .05; (L) Schematic diagram. All data were expressed as the mean  $\pm$  SD of triplicate experiments. In each independent experiment, the sample size for each group of experiments is 3.

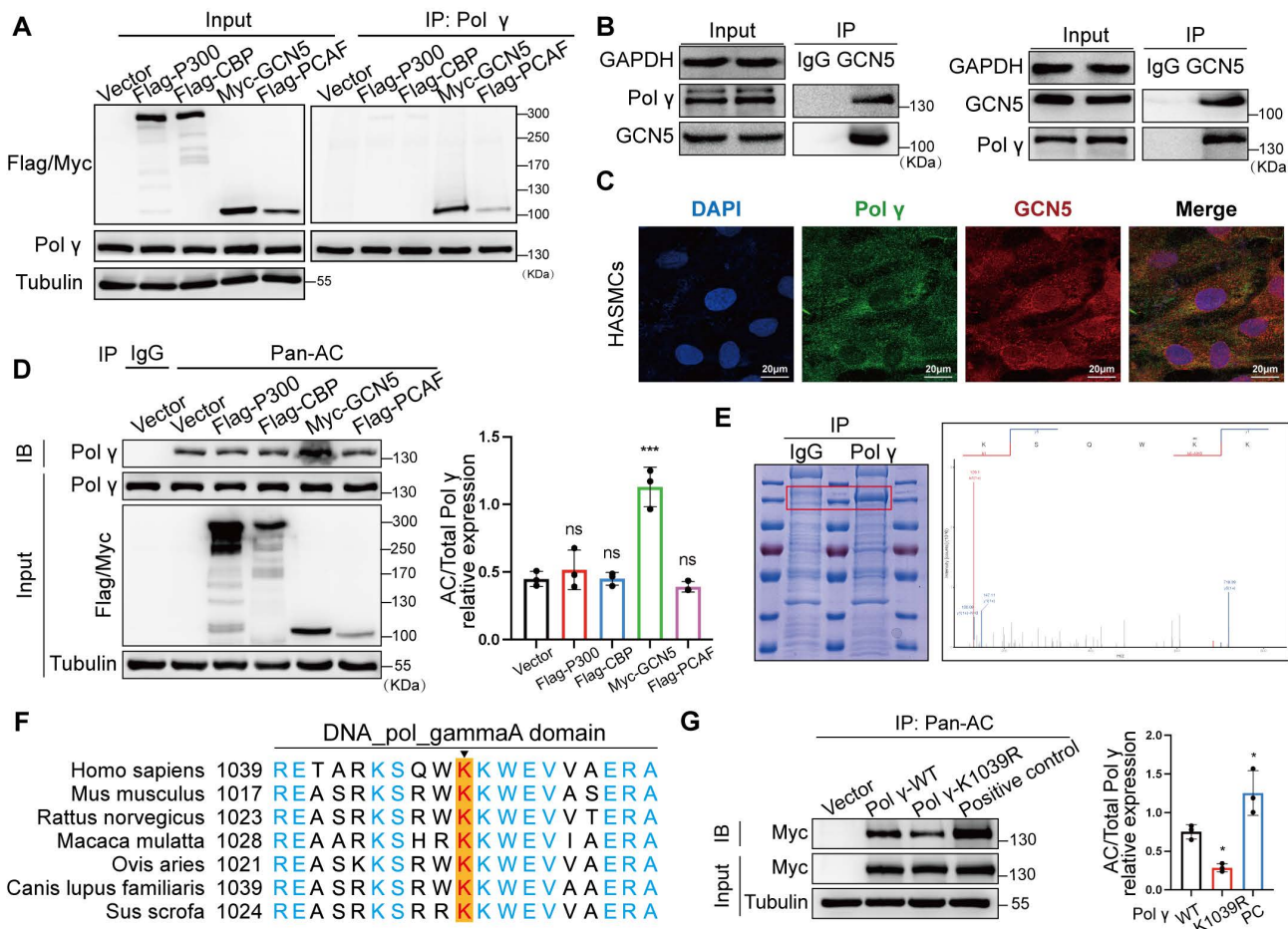


**Figure 3. GCN5 is the acetyltransferase for Poly acetylation at K1039.** (A) The Co-IP assay to screen the interaction between Poly and acetyltransferases. (B) The Co-IP assay to confirm the interaction between Poly and GCN5. (C) The interaction between Poly and GCN5 by confocal assay. (D) The effect of various acetyltransferases in acetylating Poly. Right panel is the quantification analysis. The expression of Poly in input was used as a loading control. \*\*\*p < .001, ns p > 0.05; (E) Enrich endogenous Poly and conduct mass spectrometry acetylation modification omics to confirm the acetylated site of Poly. (F) The conserved analysis of DNA sequence around K1039 site of Poly in different species. (G) The CO-IP experiment and quantification of relative acetylation level of different types of Poly. The positive control was additionally treated with TSA+NAM to inhibit deacetylation on the basis of Poly-WT transfection. The expression of Myc in input was used as a loading control. \*p < .05. Data were expressed as the mean ± SD of triplicate experiments. All data were expressed as the mean ± SD of triplicate experiments. In each independent experiment, the sample size for each group of experiments is 3.

As nicotinamide (NAM, a Sirtuins inhibitor) increased Poly acetylation while histone deacetylase (HDAC) family inhibitors trichostatin A (TSA) had no effect, we focused on the Sirtuins family (Figure 4A). The Co-IP experiment showed Sirt3 had strongest binding with Poly, which was further confirmed by endogenous Co-IP and colocalization experiments (Figure 4B-D). By acetylation modification experiments, Sirt3 emerged as the dominant deacetylase counteracting the acetylation of Poly (Figure 4E), with pharmacological agents confirming its regulatory role. Sirt3 activator reduced Poly acetylation and Sirt3 inhibitor elevated Poly acetylation (Figure 4F, G). Sirt3 had strongest deacetylation effect than other Sirtuins family deacetylases in mitochondrial and we found Sirt3 deacetylase activity deficiency mutation (H248Y) lost the effect in down-regulating Poly acetylation (Figure 4H).

These findings establish a GCN5/Sirt3-K1039 axis as the central molecular pathway modulating Poly acetylation.

### D257A mutation reduced the binding capacity of Poly with mtDNA by elevating the K1039 acetylation

The D257 residue is critical for Poly function, which is evolutionarily conserved across species (Figure 5A). By *in vivo* and *in vitro* chromatin immunoprecipitation (Ch-IP) assays, we found that the D257A mutation significantly weakened Poly's binding affinity to mtDNA (Figure 5B, C). Co-IP and co-localization assays further demonstrated that this mutation disrupted the interaction between Poly and Sirt3 (Figure 5D-F), providing a mechanistic basis for the observed elevation in K1039 acetylation. Domain truncation studies coupled with Co-IP experiments

localized Sirt3's binding region to the DNA\_POL\_gammaA domain of Poly (Figure 5G, H). Protein spatial structure prediction revealed close proximity between the DNA\_POL\_gammaA domain and the D257 residue (Figure 5I), suggesting that the D257A mutation induced conformational changes that impair Sirt3 binding. Building on our structural analyses, we employed molecular docking to evaluate how the D257A mutation influenced the Poly-Sirt3 interface. Our simulations revealed that this mutation induced a marked conformational rearrangement in Poly structure. While the primary binding site remained structurally intact, the mutation substantially reduced binding affinity between Poly and Sirt3. These observations suggested that D257A

allosterically altered the interfacial dynamics, compromising the Poly-Sirt3 interaction through indirect structural effects rather than direct disruption of the binding motif (Figure S1). Subsequent Co-IP assays confirmed that the D257A mutation universally reduced Poly-Sirt3 interaction, independent of the K1039 site's acetylation status (Figure 5J, K). Ch-IP experiments corroborated these findings that D257A diminished mtDNA binding in Poly-WT and K1039R, while the K1039Q mutant retained normal mtDNA association (Figure 5L). Collectively, these results establish a model wherein D257A disrupted Poly-Sirt3 interaction, leading to hyperacetylation at K1039 (Figure 5M).

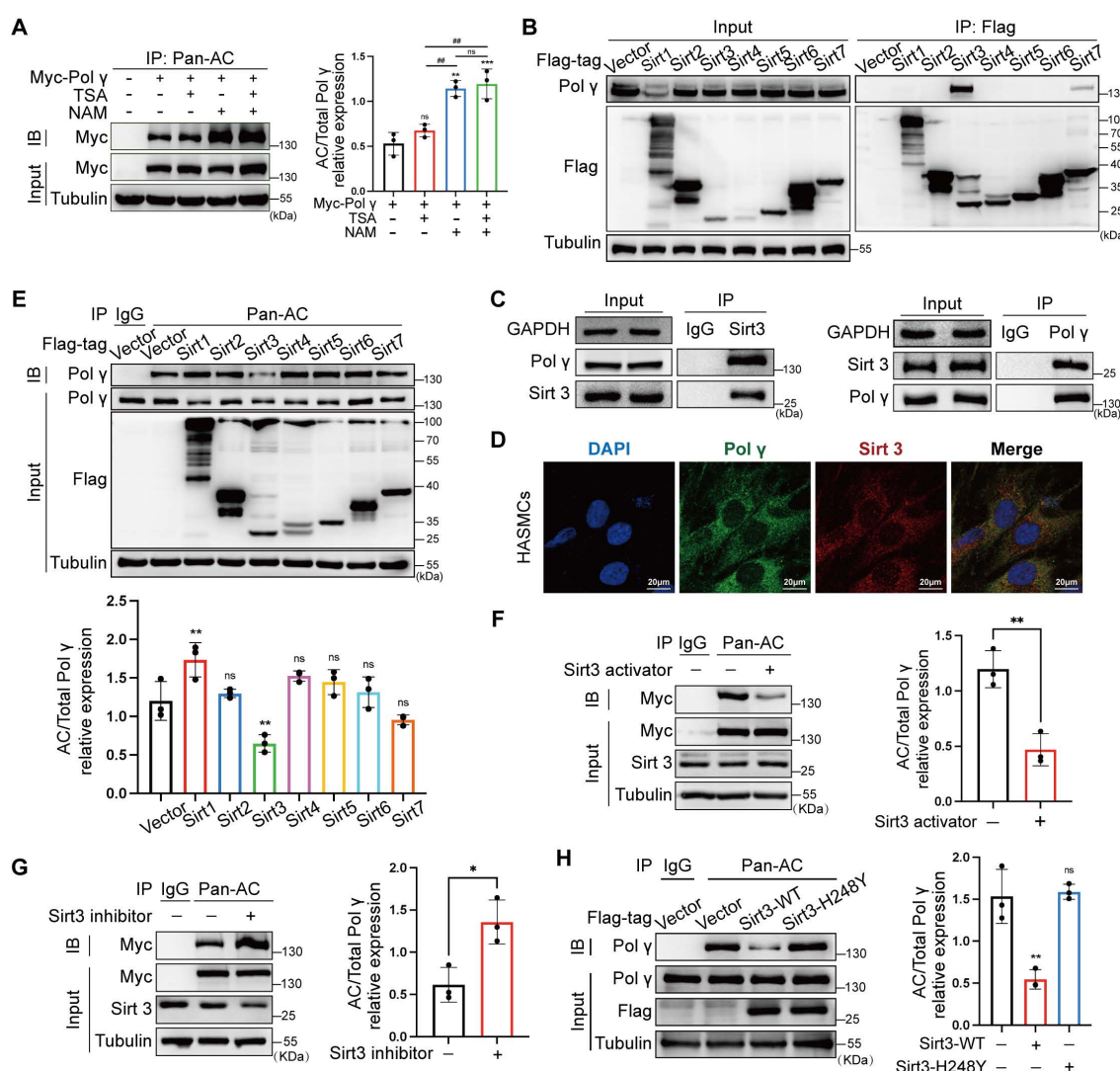


**Figure 4. Sirt3 serves as deacetylase in Poly acetylation.** (A) The Co-IP assay and quantification analysis of relative acetylation level of Poly. The HASMC was treated with TSA/NAM for 24 hours. The expression of Myc in input was used as a loading control. \*\*\*p < .001, \*\*p < .01, #p < .01, ns p > 0.05; (B) Screen the interaction between Poly and various deacetylases by Co-IP assay; (C) Confirm the interaction between Poly and Sirt3 by Co-IP assay; (D) Confirm the interaction between Poly and Sirt3 by confocal assay; (E) Compare the capacity of various deacetylases in deacetylating Poly. The bottom is the quantification analysis. The expression of Poly in input was used as a loading control. \*\*p < .01, ns p > 0.05; (F-G) Detect the acetylation level of Poly with treatment of Sirt3 activator (F) or Sirt3 inhibitor (G) in HASMCs by Co-IP assay. The right panel is the relative quantification analysis. \*\*p < .01, \*p < .05; (H) The Co-IP experiment and quantification of relative acetylation level of Poly, the HASMC was transfected with Sirt3 and deacetylase activity deficiency Sirt3 (H248Y). The expression of Myc in input was used as a loading control. \*p < .05. All data were expressed as the mean ± SD of triplicate experiments. In each independent experiment, the sample size for each group of experiments is 3.

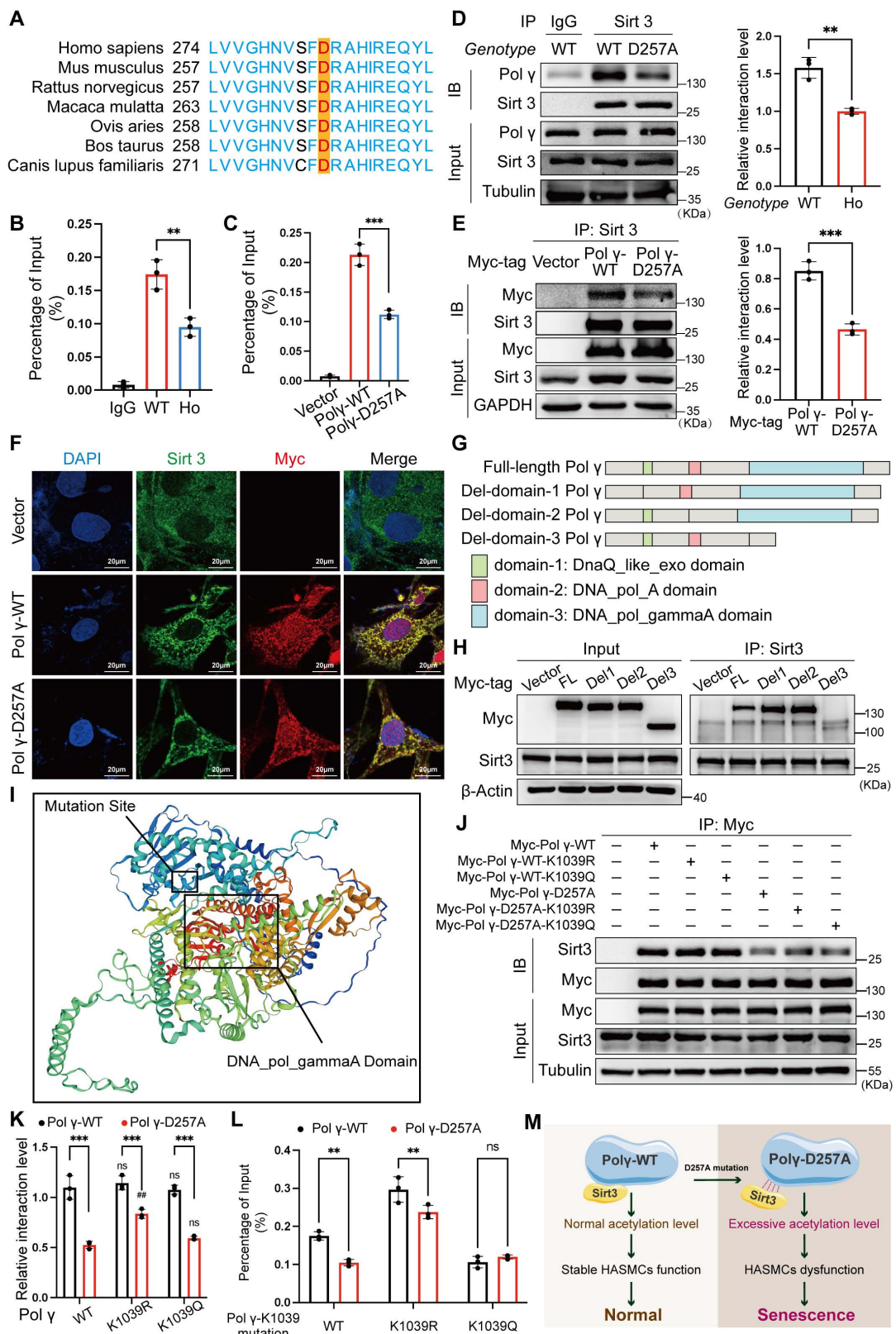


**Figure 5. D257A mutation impairs poly polymerase activity via enhanced K1039 acetylation.** (A) The conserved analysis of DNA sequence around D257 site of Poly in different species; (B-C) The Ch-IP experiments to evaluate the binding degree between Poly and mtDNA *in vivo* (B) and *in vitro* (C). WT for *POLG*<sup>WT/WT</sup> mice and HO for *POLG*<sup>D257A/D257A</sup> mice. \*\*\*p < .001, \*\*p < .01; (D-E) Compare the interaction between Sirt3 and different types of Poly *in vivo* (D) and *in vitro* (E) by Co-IP assay. The right panel is quantification analysis. \*\*\*p < .001, \*\*p < .01; (F) Compare the interaction between Sirt3 and different types of Poly by confocal; (G) Schematic diagram of domain-deletion plasmid of Poly; (H) Clarify the interaction domain of Poly with Sirt3 by Co-IP assay; (I) The predictive 3D structure of Poly by SWISS-MODEL; (J-K) The Co-IP experiment and quantification analysis to evaluate the interaction degree between Sirt3 and different types of Poly. \*\*\*p < .001, \*\*p < .01, #p < .01, ns p > 0.05; (L) Evaluate the binding degree between different types of Poly and mtDNA by Ch-IP assay. \*\*p < .01, ns p > 0.05; (M) Schematic diagram. All data were expressed as the mean  $\pm$  SD of triplicate experiments. In each independent experiment, the sample size for each group of experiments is 3.

These findings highlight a critical regulatory axis linking functional integrity of Poly, Sirt3-mediated deacetylation, and mtDNA maintenance. By using *POLGD257A/D257A* premature aging mice, demonstrating the broad applicability of this novel regulatory mechanism across multiple biological systems, providing critical insights into the molecular basis of age-related functional decline.

### Hyper-acetylation at K1039 drives senescence via mitochondrial and functional deficits

To investigate the functional impact of Poly acetylation at K1039, we transfected HASMCs with wild type Poly (Poly-WT), acetylation deficiency mimetic Poly-K1039R or hyper acetylation mimetic Poly-K1039Q. Overexpression of Poly-WT enhanced HASMCs contractility, an effect further amplified by the K1039R mutation. In contrast, Poly-K1039Q failed to augment contractility compared to the vector control (Figure 6A). WB revealed that Poly-WT upregulated contractile markers LCP and TRPC6, with Poly-K1039R exhibiting stronger induction, while Poly-K1039Q showed no effect (Figure 6B, C). We found that Poly promoted cell proliferation, intriguingly, Poly-K1039Q also induced hyperproliferation, whereas Poly-K1039R only modestly increased proliferation (Figure 6D). Metabolically, Poly-WT elevated CS expression and suppressed PKM2 phosphorylation, promoting oxidative phosphorylation. These effects were enhanced by Poly-K1039R but absent in Poly-K1039Q-transfected cells (Figure 6E-G). In terms of mitochondrial homeostasis, we found that the MMP and functional integrity were robustly enhanced by Poly-WT and further augmented by Poly-K1039R, but only marginally improved by Poly-K1039Q (Figure 6H, I). To assess binding capacity of Poly, we performed Ch-IP assays to quantitatively measure the binding affinity between Poly and mtDNA, which allowed us to establish a robust correlation between Poly-mtDNA interaction dynamics. Ch-IP assays confirmed that Poly-K1039R strengthened Poly-mtDNA binding, while Poly-K1039Q diminished this interaction (Figure 6J). To elucidate mechanistic insight into how K1039 acetylation regulates the mtDNA-binding capacity of Poly, we performed structural predictions using AlphaFold. We chose and analyzed five independent models consistently revealed that K1039 acetylation induced significant substantial conformational rearrangements in Poly, characterized by a transition from a compact to a more relaxed structural state. This acetylation-dependent structural relaxation likely impairs the precise spatial coordination required for effective mtDNA binding (Figure S2).

Herein, we propose a Poly-mtDNA binding capacity-mitochondrial function-cellular function and fate regulatory axis. This axis delineates how Poly modulates mitochondrial homeostasis via its acetylation, thereby dictating cellular phenotypes such as contraction or senescence (Figure 6K). Collectively, deacetylated Poly could ensure the binding of Poly to mtDNA, sustain mitochondrial oxidative metabolism, preserve the contractile phenotype of HASMCs, and prevent from senescence.

### K1039 deacetylation is essential for Poly in maintaining mitochondrial homeostasis and HASMC function

To validate the causal role of K1039 acetylation in maintaining the HASMCs function and mitochondrial homeostasis, we performed rescue experiments in Poly-knockdown (Sh-Poly) HASMCs cell line. Poly deficiency impaired contractility, which was fully restored by Poly-WT and maximally rescued by Poly-K1039R, while Poly-K1039Q exhibited negligible rescue which was akin to negative controls (NC) (Figure 7A, B). Similarly, WB results showed that Poly-K1039Q failed to upregulate expression of LCP and TRPC6, while Poly-WT and Poly-K1039R robustly increased their expression (Figure 7C, D). Poly deficiency obviously decreased the proliferation of HASMCs and overexpression of Poly restored fully its proliferation. Strikingly, Poly-K1039Q exacerbated hyperproliferation in Sh-Poly HASMCs, whereas Poly-K1039R normalized proliferation to NC levels (Figure 7E). Metabolic profiling showed that Poly deficiency reduced CS expression and elevated p-PKM2 level, indicative of glycolytic dominance. In rescue experiments, Poly-WT and Poly-K1039R restored CS levels and suppressed p-PKM2, but Poly-K1039Q had minimal effect (Figure 7F). These results indicated it was deacetylated Poly that ensured metabolic homeostasis which was indicative of aerobic respiration dominance. Except for comprehensive metabolic pathway analysis, mitochondrial membrane potential dynamics were quantitatively monitored to evaluate role of acetylated Poly in maintain mitochondrial homeostasis and determinate mitochondrial fate. JC-10 assays mirrored these trends that Poly deficiency markedly reduced MMP, thereby severely compromising mitochondrial integrity and homeostatic maintenance as previous results. But Sh-Poly-induced mitochondrial dysfunction was fully rescued by Poly-WT and Poly-K1039R, especially the Poly-K1039R had maximally rescue effect, while Poly-K1039Q provided partial recovery (Figure 7G, H).

These findings demonstrated K1039

deacetylation was essential for sustaining Poly's mtDNA-binding capacity. Elevated acetylation at the K1039 residue inversely correlates with Poly binding capacity with mtDNA and molecular function.

Hyperacetylation at K1039 disrupted mtDNA binding, impaired oxidative metabolism, and driven HASMCs toward a proliferative, senescence-prone phenotype (Figure 7I).

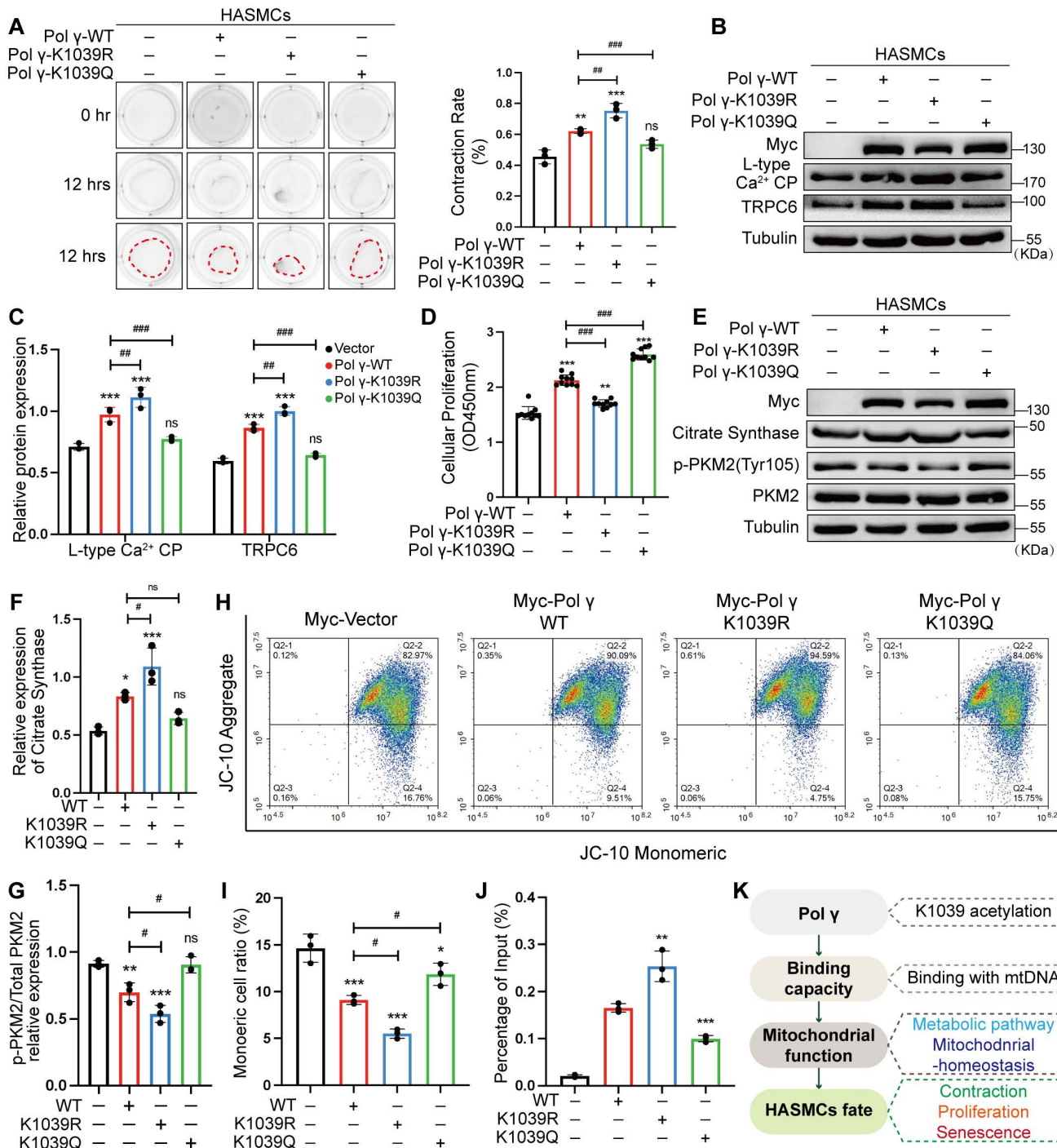


**Figure 6. Acetylated Poly regulates HASMC function and mitochondrial homeostasis via mtDNA binding.** (A) Evaluate the effect of different acetylated Poly in contractive ability by collagen gel contraction experiment. The percentage of gel surface area contraction (%) was calculated using the formula:  $[(0\text{h area} - 12\text{h area}) / 0\text{h area}] \times 100\%$ . \*\*\*p < .001, \*\*p < .01, \*\*\*p < .001, ##p < .01, ns p > 0.05; (B-C) Transfect the HASMCs with various acetylated Poly and compare the expression of L-type Ca<sup>2+</sup> CP and TRPC6. The expression of Tubulin was used as a loading control. \*\*\*p < .001, \*\*\*p < .001, \*\*\*p < .001, ##p < .01, ns p > 0.05; (D) Compare the proliferation alteration of HASMCs after transfecting various acetylated Poly by CCK-8 assay. \*\*\*p < .001, \*\*p < .01, \*\*\*p < .001; (E-G) Conduct WB analysis and quantification analysis to evaluate protein expression (citrate synthase, p-PKM2, PKM2, Tubulin) in HASMC which were transfected with different acetylated Poly. The expression of Tubulin was used as a loading control for citrate synthase, and PKM2 was used as a loading control for p-PKM2. \*\*\*p < .001, #p < .05, ns p > 0.05; (H-I) The MMP alteration under various acetylated Poly conditions by JC-10 assay. Compare the difference of monomeric cells ratio (green) in every subgroup. \*\*\*p < .001, \*p < .05, #p < .05; (J) The binding degree between different acetylated Poly and mtDNA by Ch-IP assay. \*\*\*p < .001, \*\*p < .01; (K) Schematic diagram. All data were expressed as the mean  $\pm$  SD of triplicate experiments. In each independent experiment, the sample size for each group of experiments is 3.

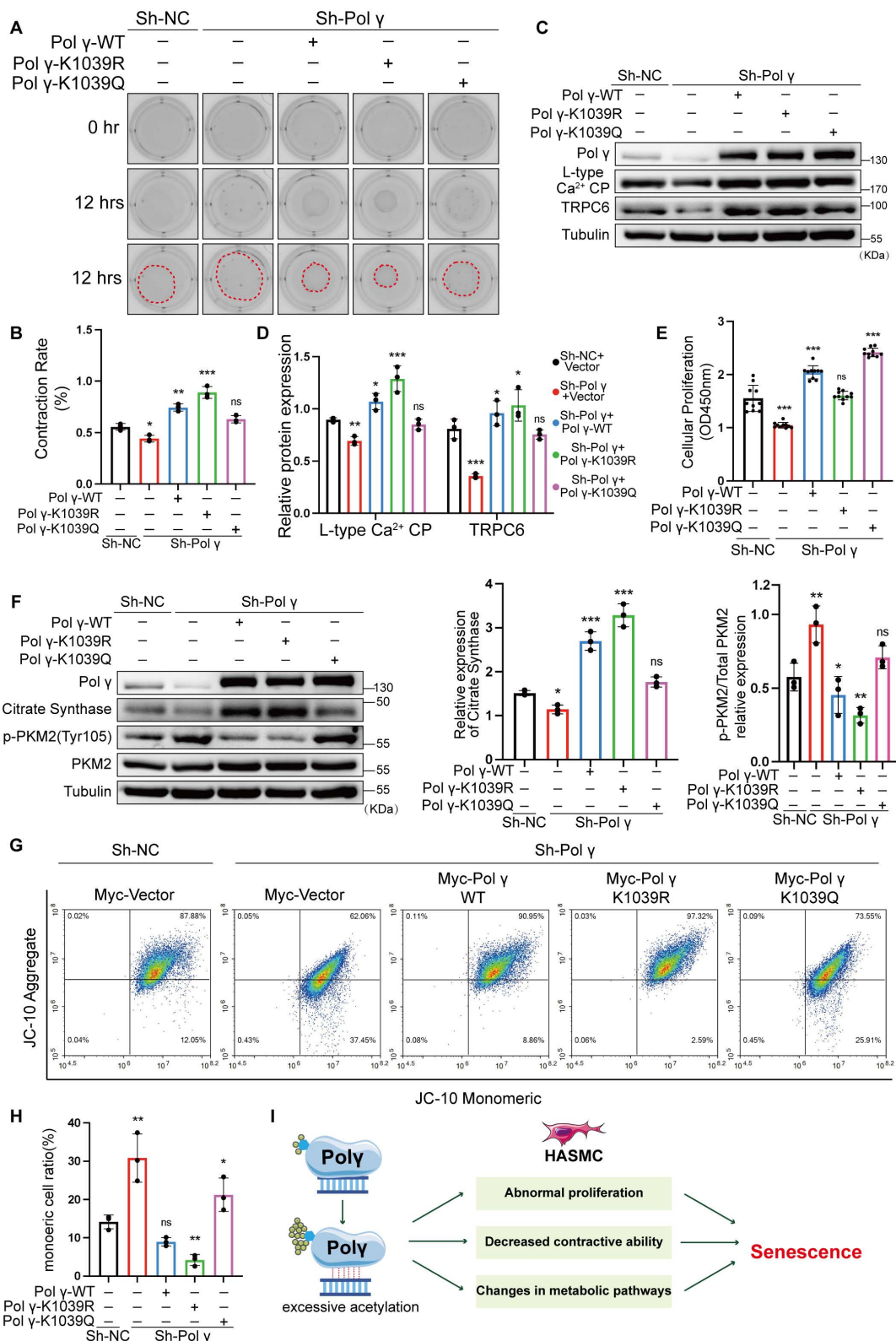


**Figure 7. K1039 acetylation status governs Poly's role in metabolic and functional rescue.** (A-B) Transfect Sh-Poly-HASMCs with various acetylated Poly condition plasmid, evaluating the contractive ability by collagen gel contraction experiment. The percentage of gel surface area contraction (%) was calculated using the formula: [(0h area - 12h area) / 0h area] × 100%. \*\*\*p < .001, \*\*p < .01, \*p < .05, ns p > 0.05; (C-D) Knock-down the expression of Poly in HASMCs and rescue with various acetylated Poly and compare the expression of L-type Ca<sup>2+</sup> CP and TRPC6. The expression of Tubulin was used as a loading control. \*\*\*p < .001, \*\*p < .01, \*p < .05, ns p > 0.05; (E) Evaluate the rescue effect of different acetylated Poly in regulating the proliferation effect by CCK-8 assay. The results are defined as the absorbance in 450nm. \*\*\*p < .001, ns p > 0.05; (F) Conduct WB analysis and quantification analysis to evaluate protein expression (citrate synthase, p-PKM2, PKM2, Tubulin) in Sh-Poly-HASMC which were transfected with different acetylated Poly plasmids for 48 hours. The expression of Tubulin was used as a loading control for citrate synthase, and PKM2 was used as a loading control for p-PKM2. \*\*\*p < .001, \*\*p < .01, \*p < .05, ns p > 0.05; (G-H) The JC-10 assay to evaluate rescue effect of different acetylated Poly in regulating MMP. Compare the difference of monomeric cells ratio (green) in every subgroup. \*\*p < .01, \*p < .05, ns p > 0.05; (I) Schematic diagram. All data were expressed as the mean ± SD of triplicate experiments. In each independent experiment, the sample size for each group of experiments is 3.

## Discussion

Here, our study established a conceptual advance in Poly functional regulation by demonstrating that acetylation fundamentally modulated its mtDNA binding capacity. We demonstrate that Poly undergoes GCN5/Sirt3-mediated acetylation at K1039, which was markedly enhanced during cellular senescence. Acetylation of K1039 attenuates Poly binding to mtDNA, impairing mitochondrial function and driving both functional decline and senescence in HASMCs. Strikingly, hyperacetylation of K1039 or introduction of D257A mutation reduced the binding between Poly and mtDNA, compromised mitochondrial integrity, and ultimately precipitated HASMC senescence through loss of contractile capacity.

As a critical mitochondrial regulator, POLG governs cellular fate by maintaining mitochondrial functional homeostasis and ATP balance[19-21]. This is particularly vital in high-energy-demand tissues such as muscle and brain, consequently, POLG deficiency frequently manifest as myopathies and neuropathies, such as activation of neurotoxic astrocytes and peripheral neuropathy[21-24]. In 2001, pioneering work by Van Goethem *et al.* identified four *POLG* mutations in patients with progressive external ophthalmoplegia (PEO), establishing a causal link between Poly deficiency and disease [25]. Subsequently, mutations in *POLG* were discovered in patients with ataxia [26-28]. Furthermore, *POLG* mutations were confirmed as the cause of Alpers-Huttenlocher syndrome (AHS), marking a seminal breakthrough in understanding the molecular basis of this *POLG*-related disorder[29, 30]. However, it is particularly noteworthy that limited evidence from clinical disorders or mechanistic studies implicated reduced Poly expression as the primary cause of mitochondrial functional collapse. Instead, various large-scale clinical analyses have confirmed the pathogenic mechanism predominantly arisen from mutations that impair catalytic activities of Poly [4]. Consistent with this, the D257A mutation animal model employed in this study similarly exhibited unchanged Poly expression, but displayed a 5-fold increase in mtDNA defect [15, 16, 31]. Although these mutations took place across various domains and involve multiple amino acid residues, they uniformly resulted in mtDNA defects and depletion. This feature strongly suggested that all pathogenic *POLG* mutations ultimately impair its polymerase or exonuclease activities, leading to catastrophic mtDNA failure. This phenomenon supported our hypothesis that Poly acted as a central integrator and signal

transducer for diverse mitochondrial damage signals. While some studies suggest extramitochondrial functions for Poly[32, 33], but we believed the primary pathway by which Poly deficiency altered cellular fate was through mtDNA dysregulation. Consequently, these findings strongly implied the existence of an underlying regulatory mechanism capable of precisely coordinating the POLG-mtDNA interaction.

Our findings position K1039 acetylation as a central regulator of HASMC homeostasis and senescence. While prior studies linked Poly deficiency or mutation to aging-associated pathologies[4, 5, 34], we identify elevated K1039 acetylation as a unifying molecular signature across diverse senescence models, including *POLGD257A/D257A* mice. Mechanistically, the D257A mutation disrupted Sirt3-Poly interaction, exacerbating K1039 acetylation and diminishing mtDNA binding—a prerequisite for Poly-mediated transcription of respiratory chain components[4, 35]. We propose that diverse damage signals converge on K1039 hyperacetylation to modulate Poly activity indirectly, rather than directly targeting Poly-mtDNA binding. This paradigm reconciles previous observations that both Poly depletion and catalytic impairment accelerate senescence[34, 36], positioning acetylation as a tunable regulator of mitochondrial genome maintenance. Notably, K1039 acetylation precipitated metabolic reprogramming from oxidative phosphorylation to glycolysis which is a hallmark of senescent cells. By disrupting mtDNA replication and respiratory complex assembly[37], hyperacetylated Poly forces HASMCs into an energetically inefficient glycolytic state, culminating in mitochondrial collapse. Concomitant loss of contractile function and aberrant proliferation mirrored phenotypic switching observed in vascular aging[38, 39]. Our data align with the Hayflick limit paradigm[40, 41], wherein replicative exhaustion triggers senescence, but extend this concept by implicating acetylation-driven mitochondrial failure as an accelerator of proliferative arrest.

Our current findings demonstrate that K1039 acetylation significantly impairs Poly's binding affinity for mtDNA. Given that the D257A mutation similarly weakens this interaction, we hypothesize that K1039 acetylation may modulate the exonuclease activity of Poly. This conjecture is supported by our previous work showing that the exonuclease-deficient D257A mutant triggered excessive p53 recruitment to mitochondria, where it interacted with Poly to help maintain mtDNA quality control. Collectively, our data support a model wherein impaired Poly-mtDNA binding, while not affecting intrinsic polymerase activity, disrupts mtDNA quality control in a

binding-dependent manner and ultimately leads to mitochondrial dysfunction and HASMC cellular impairment.

Furthermore, while several studies have reported decreased Poly expression in diverse pathological conditions [10, 33]. We noted that these conditions typically involve multifactorial pathological insults processes, within these complex processes, Poly dysregulation likely represented one component influenced by up-stream signaling events. This suggested that cellular fate under such pathological conditions wasn't solely determined by the Poly pathway. In contrast to these correlative observations, our study employed definitive rescue experiments. Specifically, we performed Poly knockdown followed by transfecting with various Poly plasmids (K1039K, K1039R and K1039Q), mimicking distinct acetylation states, directly established the acetylation status of Poly as the primary triggering event for mitochondrial dysfunction and cellular senescence. Technical limitations merit consideration. Structural occlusion of K1039 within Poly's folded conformation precluded development of site-specific acetyl antibodies. Residual acetylation in K1039-mutant Poly suggests auxiliary modification sites, though the profound functional impact of K1039R underscores its primacy in regulating senescence. Future studies employing Poly K1039R knock-in models will clarify the spatiotemporal dynamics of this modification in aging.

In conclusion, we delineate a GCN5/Sirt3-Poly axis wherein K1039 acetylation serves as a molecular switch governing mitochondrial fidelity and cellular aging. By linking post-translational regulation of Poly to metabolic homeostasis and phenotypic plasticity of HASMCs, our work unveils novel therapeutic opportunities for age-related vascular pathologies. This mechanistic bridge between mtDNA maintenance and protein acetylation networks establishes Poly as a linchpin target for interventions against degenerative aging.

## Supplementary Material

Supplementary figures.

<https://www.ijbs.com/v22p2435s1.pdf>

## Acknowledgements

### Funding

This study was supported by National Natural Science Foundation of China (82301778) and the China Postdoctoral Science Foundation to Pengbo Wang (#2023MD744274).

## Permission statement

All co-authors read and approved the final manuscript. Besides, all co-authors and participants have given their consent for publication of this article.

## Author contributions

LC, YXS and GZS raised the concept; PBW, KXC and LFS conducted the *in vitro* experiments; PBW, LMY and XFG conducted the *in vivo* experiments; PBW, YY, MYX, CL and TZ conducted the molecular biological experiments; PBW, NJZ and LC administrate the project; PBW, SZ, YY and XFG wrote the original draft; YXS, LC, GZS, NJZ and PBW reviewed and edited the final manuscript.

## Data availability statement

The original mass spectrometry data reported in this paper will be shared by the Prof. Yingxian Sun upon request. Any additional information required to reanalyze the data reported in this paper is available from Prof. Yingxian Sun (yxsun@cmu.edu.cn).

## Ethics approval statement

Animal protocols were approved by the Institutional Animal Care and Use Committee (IACUC) of China Medical University and conducted in compliance with NIH guidelines (Publication No. 85-23, revised 1985).

## Competing Interests

The authors have declared that no competing interest exists.

## References

1. Rutledge J, Oh H, Wyss-Coray T. Measuring biological age using omics data. *Nat Rev Genet.* 2022; 23: 715-27.
2. Lacolley P, Regnault V, Segers P, Laurent S. Vascular Smooth Muscle Cells and Arterial Stiffening: Relevance in Development, Aging, and Disease. *Physiol Rev.* 2017; 97: 1555-617.
3. Bennett MR, Sinha S, Owens GK. Vascular Smooth Muscle Cells in Atherosclerosis. *Circ Res.* 2016; 118: 692-702.
4. Rahman S, Copeland WC. POLG-related disorders and their neurological manifestations. *Nat Rev Neurol.* 2019; 15: 40-52.
5. Stumpf JD, Saneto RP, Copeland WC. Clinical and molecular features of POLG-related mitochondrial disease. *Cold Spring Harb Perspect Biol.* 2013; 5: a011395.
6. Carroll J, He J, Ding S, Fearnley IM, Walker JE. Persistence of the permeability transition pore in human mitochondria devoid of an assembled ATP synthase. *Proc Natl Acad Sci U S A.* 2019; 116: 12816-21.
7. Wang P, Wu B, You S, Lu S, Xiong S, Zou Y, et al. DNA Polymerase Gamma Recovers Mitochondrial Function and Inhibits Vascular Calcification by Interacted with p53. *Int J Biol Sci.* 2022; 18: 409-25.
8. Fox R, Kim HS, Reddick RL, Kujoth GC, Prolla TA, Tsutsumi S, et al. Mitochondrial DNA polymerase editing mutation, PolgD257A, reduces the diabetic phenotype of Akita male mice by suppressing appetite. *Proc Natl Acad Sci U S A.* 2011; 108: 8779-84.
9. Yu E, Calvert PA, Mercer JR, Harrison J, Baker L, Figg NL, et al. Mitochondrial DNA damage can promote atherosclerosis independently of reactive oxygen species through effects on smooth muscle cells and monocytes and correlates with higher-risk plaques in humans. *Circulation.* 2013; 128: 702-12.
10. Yang Y, Li X, Xiao S, Wei Q, Ren L, Yao Y, Liu N. PARylation of POLG Mediated by PARP1 Accelerates Ferroptosis-Induced Vascular Calcification via Activating Adora2a/Rap1 Signaling. *Arterioscler Thromb Vasc Biol.* 2025; 45: 1175-91.

11. Zhang N, Zhang Y, Wu B, Wu S, You S, Lu S, et al. Deacetylation-dependent regulation of PARP1 by SIRT2 dictates ubiquitination of PARP1 in oxidative stress-induced vascular injury. *Redox Biol.* 2021; 47: 102141.
12. Zhang N, Zhang Y, Miao W, Shi C, Chen Z, Wu B, et al. An unexpected role for BAG3 in regulating PARP1 ubiquitination in oxidative stress-related endothelial damage. *Redox Biol.* 2022; 50: 102238.
13. Bai N, Li N, Cheng R, Guan Y, Zhao X, Song Z, et al. Inhibition of SIRT2 promotes APP acetylation and ameliorates cognitive impairment in APP/PS1 transgenic mice. *Cell Rep.* 2022; 40: 111062.
14. Baeza J, Smallegan MJ, Denu JM. Mechanisms and Dynamics of Protein Acetylation in Mitochondria. *Trends Biochem Sci.* 2016; 41: 231-44.
15. Trifunovic A, Wredenberg A, Falkenberg M, Spelbrink JN, Rovio AT, Bruder CE, et al. Premature ageing in mice expressing defective mitochondrial DNA polymerase. *Nature.* 2004; 429: 417-23.
16. Kujoth GC, Hiona A, Pugh TD, Someya S, Panzer K, Wohlgemuth SE, et al. Mitochondrial DNA mutations, oxidative stress, and apoptosis in mammalian aging. *Science.* 2005; 309: 481-4.
17. Huang X, Guo J, Ning A, Zhang N, Sun Y. BAG3 promotes proliferation and migration of arterial smooth muscle cells by regulating STAT3 phosphorylation in diabetic vascular remodeling. *Cardiovasc Diabetol.* 2024; 23: 140.
18. Zhang N, Zhang Y, Xu J, Wang P, Wu B, Lu S, et al.  $\alpha$ -myosin heavy chain lactylation maintains sarcomeric structure and function and alleviates the development of heart failure. *Cell Res.* 2023; 33: 679-98.
19. Manini A, Abati E, Comi GP, Corti S, Ronchi D. Mitochondrial DNA homeostasis impairment and dopaminergic dysfunction: A trembling balance. *Ageing Res Rev.* 2022; 76: 101578.
20. Moore TM, Zhou Z, Strumwasser AR, Cohn W, Lin AJ, Cory K, et al. Age-induced mitochondrial DNA point mutations are inadequate to alter metabolic homeostasis in response to nutrient challenge. *Aging Cell.* 2020; 19: e13166.
21. Lim EW, Handzlik MK, Trefts E, Gengatharan JM, Pondevida CM, Shaw RJ, Metallo CM. Progressive alterations in amino acid and lipid metabolism correlate with peripheral neuropathy in Polg(D257A) mice. *Sci Adv.* 2021; 7: eabj4077.
22. Liang KX, Chen A, Kianian A, Kristiansen CK, Yangzom T, Furriol J, et al. Activation of Neurotoxic Astrocytes Due to Mitochondrial Dysfunction Triggered by POLG Mutation. *Int J Biol Sci.* 2024; 20: 2860-80.
23. Bugiardini E, Poole OV, Manole A, Pittman AM, Horga A, Hargreaves I, et al. Clinicopathologic and molecular spectrum of RNASEH1-related mitochondrial disease. *Neurol Genet.* 2017; 3: e149.
24. Wong LJ, Naviaux RK, Brunetti-Pierri N, Zhang Q, Schmitt ES, Truong C, et al. Molecular and clinical genetics of mitochondrial diseases due to POLG mutations. *Hum Mutat.* 2008; 29: E150-72.
25. Van Goethem G, Dermaut B, Löfgren A, Martin JJ, Van Broeckhoven C. Mutation of POLG is associated with progressive external ophthalmoplegia characterized by mtDNA deletions. *Nat Genet.* 2001; 28: 211-2.
26. Van Goethem G, Luoma P, Rantamäki M, Al Memar A, Kaakkola S, Hackman P, et al. POLG mutations in neurodegenerative disorders with ataxia but no muscle involvement. *Neurology.* 2004; 63: 1251-7.
27. Van Goethem G, Martin JJ, Dermaut B, Löfgren A, Wibail A, Verkerken D, et al. Recessive POLG mutations presenting with sensory and ataxic neuropathy in compound heterozygote patients with progressive external ophthalmoplegia. *Neuromuscul Disord.* 2003; 13: 133-42.
28. Hakonen AH, Heiskanen S, Juvonen V, Lappalainen I, Luoma PT, Rantamaki M, et al. Mitochondrial DNA polymerase W748S mutation: a common cause of autosomal recessive ataxia with ancient European origin. *Am J Hum Genet.* 2005; 77: 430-41.
29. Naviaux RK, Nguyen KV. POLG mutations associated with Alpers' syndrome and mitochondrial DNA depletion. *Ann Neurol.* 2004; 55: 706-12.
30. Naviaux RK, Nguyen KV. POLG mutations associated with Alpers syndrome and mitochondrial DNA depletion. *Ann Neurol.* 2005; 58: 491.
31. Fuke S, Kametani M, Yamada K, Kasahara T, Kubota-Sakashita M, Kujoth GC, et al. Heterozygous Polg mutation causes motor dysfunction due to mtDNA deletions. *Am J Clin Transl Neurol.* 2014; 1: 909-20.
32. Lv M, Zhang S, Dong Y, Cao L, Guo S. PolG Inhibits Gastric Cancer Glycolysis and Viability by Suppressing PKM2 Phosphorylation. *Cancer Manag Res.* 2021; 13: 1559-70.
33. Zhu Y, Zhang JL, Yan XJ, Ji Y, Wang FF. Exploring a new mechanism between lactate and VSMC calcification: PARP1/POLG/UCP2 signaling pathway and imbalance of mitochondrial homeostasis. *Cell Death Dis.* 2023; 14: 598.
34. Liang KX, Kristiansen CK, Mostafavi S, Vatne GH, Zantingh GA, Kianian A, et al. Disease-specific phenotypes in iPSC-derived neural stem cells with POLG mutations. *EMBO Mol Med.* 2020; 12: e12146.
35. Foote K, Reinhold J, Yu EPK, Figg NL, Finigan A, Murphy MP, Bennett MR. Restoring mitochondrial DNA copy number preserves mitochondrial function and delays vascular aging in mice. *Aging Cell.* 2018; 17: e12773.
36. Bakthavatchalu V, Dey S, Xu Y, Noel T, Jungsuwadee P, Holley AK, et al. Manganese superoxide dismutase is a mitochondrial fidelity protein that protects Poly against UV-induced inactivation. *Oncogene.* 2012; 31: 2129-39.
37. Graziewicz MA, Longley MJ, Copeland WC. DNA polymerase gamma in mitochondrial DNA replication and repair. *Chem Rev.* 2006; 106: 383-405.
38. Herranz N, Gil J. Mechanisms and functions of cellular senescence. *J Clin Invest.* 2018; 128: 1238-46.
39. Calcinotto A, Kohli J, Zagato E, Pellegrini L, Demaria M, Alimonti A. Cellular Senescence: Aging, Cancer, and Injury. *Physiol Rev.* 2019; 99: 1047-78.
40. Shay JW, Wright WE. Hayflick, his limit, and cellular ageing. *Nat Rev Mol Cell Biol.* 2000; 1: 72-6.
41. Gadalla SM, Aubert G, Wang T, Haagenson M, Spellman SR, Wang L, et al. Donor telomere length and causes of death after unrelated hematopoietic cell transplantation in patients with marrow failure. *Blood.* 2018; 131: 2393-8.